Light assisted synthesis of poly-para-phenylene on Ag(001)

Veronique Langlais, Kathrin Schneider, Hao Tang

Light assisted synthesis of poly-para-phenylene on Ag(001)

V Langlais[1], K Schneider[1] and H Tang[1]

[1]CEMES-CNRS
Center for Materials Elaboration and Structural Studies,
29, rue Jeanne Marvig, BP 94347,
31055 Toulouse Cedex 4, France

E-mail: veronique.langlais@cemes.fr

Received xxxxxx
Accepted for publication xxxxxx
Published xxxxxx

Abstract

A detailed study of poly-para-phenylene obtained by light-assisted on-surface-synthesis on Ag(100) was carried out by Scanning Tunneling Microscopy and Spectroscopy together with Density Functional Theory calculations. The use of light in combination with heat allows to lower by 50 K annealing temperature the each stage of the Ullmann coupling. Debromination of the 4,4'' dibromo-p-terphenyl precursors was thus realized at 300 K, the formation of the first oligomers from the organometallic intermediate by silver bridging atom release at 423 K and poly-para-phenylene by complete elimination of the silver at 473 K. This approach to lower the reaction temperature permits to enhance the Ag(100) surface reactivity to become comparable to that of Cu(111). The underlying mechanism of light effect was proposed to occur via surface mediated excitation, with the creation of photoexcited electrons known as hot electrons correlated with surface plasmon excitation. This original pathway combining both light and heat provides an additional parameter to control on-surface-synthesis by separating the precursor activation stage from the diffusion.

Keywords: light, on-surface-synthesis, hot electrons, surface plasmon, poly-para-phenylene

1. Introduction

Poly-para-phenylene (PPP) has been considered for long as the prototype of organic semiconductor conjugated polymers and could be also seen as the narrowest graphene nanoribbon (GNR). In its neutral form, PPP is a large band gap semiconductor that can be doped to increase its conductivity, moreover, its mechanical properties, low density and high stability regarding temperature, oxygen exposure and moisture make PPP a promising candidate for organic electronics [1]. Numerous approaches to synthesize it in wet chemistry were reported [2,3]. Finally, the chemical pathway to access this long-desired polymer in its pristine form was only established in 2016 [4].

On the other hand, PPP can be also regarded as a model system for on-surface-synthesis (OSS). During the past decade, this approach has gained increasing research attention, since new molecular species and nanoarchitectures not achievable by conventional wet chemistry can be successfully formed by chemical reactions directly onto surfaces [5–13]. OSS is based on the use of a substrate not only as physical support but also as active catalyst component to initiate a chemical reaction from precursors that moreover could be carried out in an ultra-clean environment such as ultrahigh vacuum (UHV). This provides the great advantages to give access to a larger range of temperatures than in solution, to provide structural order to achieve atomic scale precision thanks to 2D confinement, to carry out chemical reactions in a solvent free environment and to benefit of additional parameters such as nanostructuration of the surface to further

confine the reaction and the reactants [14]. Up to date, a large number of reactions such as Ullmann coupling [15], Glaser coupling [16], Bergman reaction [17], aryl–aryl dehydrogenation [18], Diels–Alder reaction [19], Schiff-base reaction [20], boronic acid condensation [21], cyclotretramerization [22], etc. have been successfully performed on different metal surfaces in UHV and further investigated with the help of surface science techniques combined with theoretical calculations. The final products obtained by OSS, obviously depend on the initial molecular precursors, but are also strongly influenced by the underlying substrate, its chemical nature, its crystallographic orientation and symmetry which fully determine its reactivity. In addition, the surfaces can even directly participate with their adatoms to the formation of organometallic species (OGM). The syntheses of GNRs [23,24] and long polyacenes [25] on different metallic surfaces are definitively among the most successful and remarkable examples of OSS. Among the chemical reactions that were successfully tested on metal surfaces, Ullmann coupling is one of the most studied and one of the most popular [6,26,27]. Using Ullmann coupling, PPP has been achieved starting from various different precursors such as 1,4-diiodobenzene [28], diiodo-biphenyl and dibromo-diphenyl [29], 4,4''-dibromo-p-terphenyl [30–33]. In addition, wider nanoribbons were also on-surface synthesized from PPP by dehydrogenation and C-C coupling [34]. Belonging to the same family class, hyperbenzene and zigzag poly-m-phenylene were also successfully achieved from halogen functionalized-m-terphenyl precursors [35,36]. This process can be described as follows: after halogenated precursors adsorption onto a surface, two activation steps have to be induced: (1) radicals creation by cleavage of the C-X bond(s), with X=Cl, Br, I and (2) diffusion to provoke the chemical reaction between the reactive species. One of the key parameters to achieve covalent coupling is the temperature at which the reaction takes place. Several strategies have been imagined to lower the temperature, such as co-deposition of reactive adatoms such as Ni or Ag together with dibromo-biphenyl and diodo-biphenyl molecules on Au(111) has permitted to synthesize stable intermediates [29].

Here, an original approach was adopted combining both sun like UV-visible-near IR light and heat at each step of the Ullmann reaction towards PPP synthesis on Ag(100) and Ag(111) single crystal surfaces. The study was carried out by low temperature Scanning Tunneling Microscopy (LT-STM) and Density Functional Theory (DFT) from 4,4''-dibromo-p-terphenyl (DBTP) as precursor in order to get a detailed understanding of the mechanism of the on-surface chemical reaction assisted by light. A detailed analysis of light exposition effect at the different stages of the Ullmann reaction i.e. from self-assembly to intermediate OGM phase until complete polymerized PPP was carried out by comparing the reaction temperatures, on both surfaces yielding a lowering of the reaction temperature by 50 K and thus enhancing the surface reactivity of Ag(100) to become comparable to Cu(111). The underlying mechanism was then discussed in terms of substrate mediated electronic excitation and asymmetric energy barriers for bond cleavage and polymer formation.

2. Results and discussion

2.1 Methodology

Ag(100) and Ag(111) single crystal surfaces were prepared by cycles of Ar-sputterimg at 1 keV (ionic current ~10 μAmp) and annealing at 773 K for 30 minutes with a slow cooling down (10K/min) at the last cycle. DBTP and DITP (4,4''-diiodo-p-terphenyl) molecules were placed in a home-made mini transferable evaporator and carefully degassed until the UHV base pressure reached again the low 10-10mbar range. The cleanness of the samples and powder was checked directly in the STM. All the STM images were recorded at 5K, unless explicitly mentioned. A Xe arc discharge lamp, Oriel Newport, operating power 150 W, sun-like emission spectrum renders them a popular choice for solar simulation, was used to shine light on the samples (Fig.1SI). The emission range extends from about 200 nm to 2400 nm, with an irradiance at 0.5 m greater than 100 $mWm^{-2}nm^{-1}$ from 800 nm to 1000 nm. The experimental setup consists of an optical fiber located at the exit of the Xe arc discharge lamp together with an optical lens located in front of the UHV window to focus the photon beam on the sample surfaces. The power at the exit of the fiber was about 350 $mWm^{-2}nm^{-1}$ at 350 nm.

The density functional theory (DFT) calculations were performed by using the Vienna Ab-initio Simulation Package (VASP) [37,38]. The projector augmented wave (PAW) potentials in a plane wave basis were used to describe the valence electron ion core interaction of each element [39]. The exchange-correlation energy corresponds to that given by the Perdew-Beck-Eneker (PBE) functional within the generalized gradient approximation (GGA) [40]. The van der Waals (vdW) interactions were considered by a modified version of the semi-empirical DFT-D2 method proposed by Grimme [41]. In this version the correction was not considered for metal-metal interactions within surface slab. The kinetic energy cut-off was fixed to 440 eV, which gives a lattice parameter of 4.162 Å for the optimized fcc bulk silver (with a reciprocal lattice mesh of 15x15x15 to sample the 3D Brillouin zone). The self-consistent electronic convergence criterion was set to 10-6 eV and the geometrical relaxation was considered to be converged when the forces on each unfixed atom was lower than 0.02 eV/Å. The slab which represent the surface of Ag(001) was constructed by a 4 atomic plans with each plan contains of 48 Ag atoms (with a lateral dimension

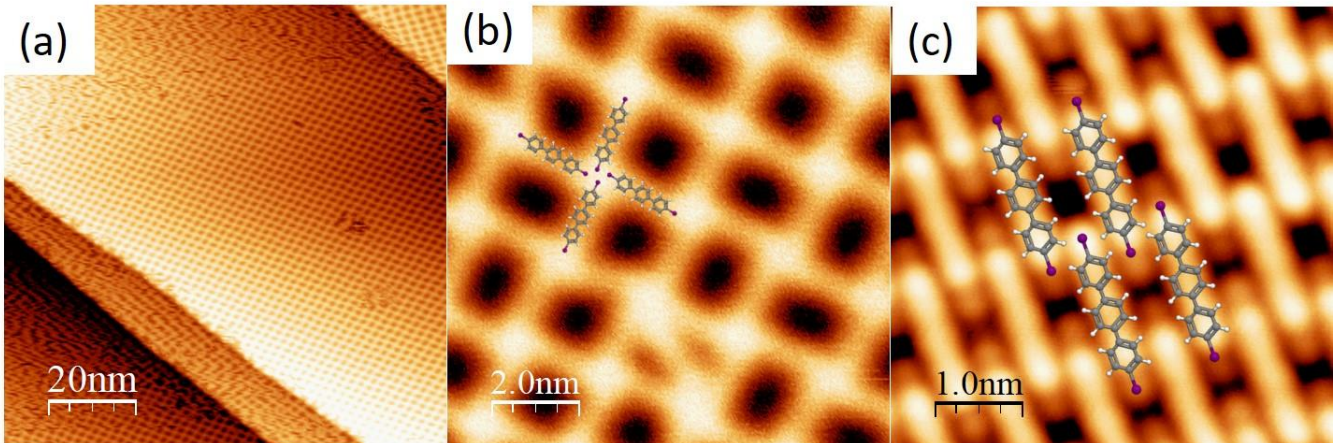

Figure 1: Constant current STM images of DBTP deposited on Ag(100) maintained at 78 K (a) bias-induced self-assembly monolayer of DBTP on Ag(100) (imaging conditions: 1 pA, 300 mV); (b) Zoom in the same area revealing halogen bonding with windmill of different chirality (imaging conditions: 1pA, 300 mV); (c) Brick-wall arrangement obtained by increasing the surface coverage. (imaging conditions: 10pA, 100 mV).

of 16.65 x 24.97 Å²), with x axis along the (100) direction and y axis along the (010) direction. The Brillouin zone was sampled with only the gamma point in the reciprocal space for preliminary calculations and a 3x3x3 k-point sampling for the electronic structure analysis. The vacuum space was set to 18.32 Å (about 12 Å from the Ag surface). The dipole correction was considered in the z direction to compensate the interface dipole effect during the energy minimization.

The activation barriers to detach iodine or bromine atom from the DITP and DBTP precursors, and to detach Ag atoms from the organometallic complexes were estimated with the transition stats obtained by using the Climbing Image Nudged Elastic Band (CI-NEB) method as implemented by the Henkelman group [42,43]. With this method, the minimum energy reaction path was identified, by optimizing the forces perpendicular to this path to be lower than 0.5 eV/Å on each of equally separated intermediate images.

2.2 Halogen bonding driven self-assembly

When deposited onto Ag(100) maintained at 78 K, DBTP formed self-assembly islands stabilized through halogen bonding, indicating that at this temperature, diffusion was high enough to allow molecular rearrangement onto the surface (fig.1a). Nevertheless, self-assembly did not take place spontaneously but was induced by rising the voltage up to a threshold bias of 1.2 V. In fig 1a, a constant current STM image recorded at 78 K revealed a pseudo square molecular reconstruction extending over the whole terraces with some disordered areas along the step edges and on narrow terraces. Noisy areas corresponding to locations where the molecules were still diffusing during the scan are also visible at the top left corner of the STM image in fig.1a. The transition between ordered and noisy areas was fuzzy and structural ordering was clearly induced by repeated scans and self-healing defects evolving with time and number of scans on the same area. Lowering the bias below the threshold value resulted in noisy STM images dominated by molecular diffusion, indicating that the reconstruction is unstable. A closest look at the nodes of the reconstruction, where a windmill shape (WM) is observed, reveals a mixture of left and right handedness giving rise to square, rectangular and trapezoidal cells. For the sake of comparison, the same experiment was conducted with DITP precursors. The stability of the molecular layer arrangement with respect to the tip bias was found to be much stronger for DITP compared to DBTP allowing scanning at lower bias without losing the structural order. These results are in good agreement with previous halogen bonding studies that have proven that the strength of the interaction is related with the increasing polarizability of the halogen (I>Br) and decreasing electronegativity [44]. Another difference worth to be mentioned is that the same chirality was found at each node of the WM arrangement yielding a perfect square arrangement (see fig2.SI). In order to elucidate the phenomenon at the origin of this bias induced molecular arrangement, a series of scans were conducted on non-ordered areas (diffusing molecules) at various tip-sample distances by approaching the tip by steps up to ΔZ=-1nm from a setpoint at 10 pA, 100 mV in order to check for electric field effect. No any order was induced by proceeding in such a way, excluding readily electric field effect on the molecular ordering. In contrast, another study on terarylene molecules on Cu(111) reporting on tip-induced formation of a supramolecular network where the 2D assembly stabilized by π-π stacking and van der Waals interactions was observed [45]. The main difference between the two systems DIPT/Ag(100) and terarylene/Cu(111) is that the dipole of the latter was found to be aligned with the vertical electric field induced by tip pulses, while in our case, the dipole would be lying rather parallel to the surface. Therefore, for our system, the ordering is energy dependent and related to a resonance of electronic states corresponding to the lowest

unoccupied state (LUMO) (see fig3.SI). By increasing the surface coverage of DBTP, a brick-wall ordering was found to become more favorable with higher density packing as shown in fig.1c. The surface area covered by unit cell in the WM arrangement was found to be about 4.81 nm^2 with 2 molecules per unit cell while the brick wall unit cell occupies about 1.6 nm^2 as well for 2 molecular units confirming the more compact structure for higher coverage [31]. This brick-wall arrangement with interconnected digits is more compact as already reported for both DBTP and DBQP on Au(111) and was also obtained for higher surface coverage. The structure is stabilized by halogen bonding as for the WM arrangement. In opposition to the WM structure, the brick wall self-assembly was not induced by tip scanning but spontaneously formed on the surface after deposition. WM on Ag(100) surface corresponds to a meta-stable configuration with a local minimum of potential energy surface (PES). This "stability" could be reached only when an additional energy was provided by applying a bias voltage during imaging.

2.3 From DBTP to PPP

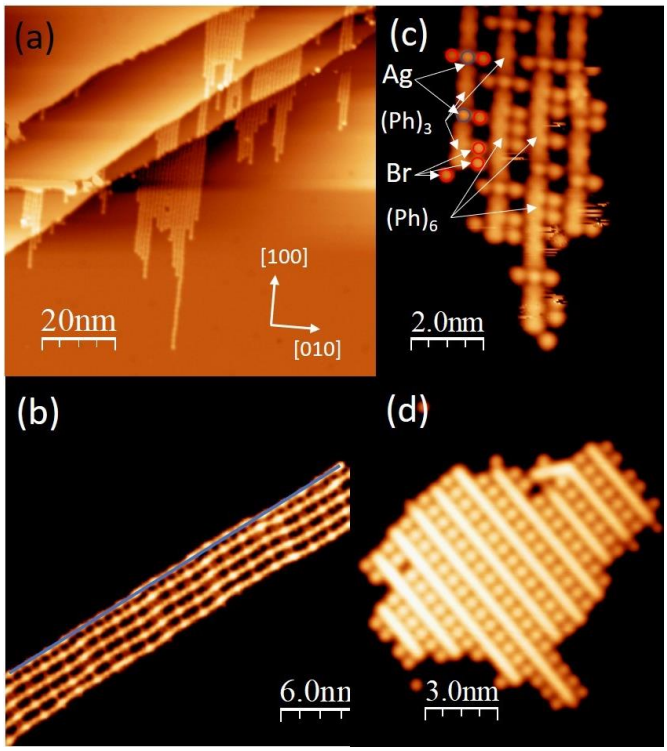

Figure 2: Current constant STM images of DBTP precursors on Ag(100) (a) light activated precursors yielding the formation of OGM intermediate phase obtained at 300K (imaging conditions: 1pA, 300 mV). (b) OGM wires along the [100] direction of the silver substrate presenting misalignment with a jump of half unit cell. (imaging conditions: 20pA, 100 mV). (c) After annealing at 423 K together light, some short oligomers start to be formed along the OGM wires by elimination of one bridging silver atom. (imaging conditions: 5pA, 30 mV). In the first row, Ag bridging atoms are depicted as blue circles and halogen atoms as red circles. (d) Completed Ullmann coupling obtained at 470 K with light exposure displaying PPP wires separated by halogen atom rows.

The DBTP precursors were then exposed to light and annealed at different temperatures to complete Ullmann coupling. At 300 K, the C-Br bonds remain intact yielding the same windmills ordering induced by tip bias as observed for the 78 K deposition. Light exposition at 300K or annealing at 340 K without light provokes debromination and generates radicals with unsaturated C-bonds which form an organometallic intermediate (OGM) by picking up adatoms from the substrate as shown in the STM overview presented in fig.2a. The Ag atoms involved in these OGM wires are either adatoms diffusing from low coordinated step edge sites, but also atoms from the substrate lattice can participate in the chain formation. The chains thus formed by alternating terphenyl groups (Ph)3 and Ag are aligned along the [100] and [010] main crystallographic directions of the substrate but some misalignment along the chains is observed provoking fluctuation along the main direction as could be seen in fig. 2b. When integrated in the OGM structure, the bridging Ag atoms are positively charged, in contrast with the halogen atoms which are negative due to charge transfer from the substrate. Therefore, along the OGM wires, the Ag atoms are very often surrounded by these negatively charged halogen atoms, which can be nevertheless, found also at other locations along the chains. After light exposition and annealing at 373 K for 3 hours, the same OGM structure was observed on the surface without noticeable change. The next stage of the on-surface Ullmann reaction consists of eliminating the bridging silvers giving rise to short oligomers obtained by light-assisted annealing at 423 K. This stage is illustrated in the high resolution STM image displayed in fig. 2c, where some $(Ph)_6$ oligomers resulting from the elimination of 1 bridging silver atom are clearly identified. In the last stage, the complete Ullmann coupling yielding PPP formation (fig. 2d) was reached for light-assisted annealing at 473 K. The PPP wires are surrounded by halogen rows and are now aligned along the <110> direction. More details on the OGM chains could be extracted from fig.3a where atomic resolution was achieved on the silver substrate. The OGM is oriented along the <100> direction and along the perpendicular <010> direction. In gas phase, the Ag-$(Ph)_3$-Ag distance was found to be d_{Ag-Ag}=1.564 nm. Experimentally, a statistical analysis of the Ag-Ag distance gave a distance d_{Ag-Ag}= 1.596 nm ± 0.02 nm, proving an adaptation of the monomer to fit the substrate lattice by stretching the C-Ag bonds. On Cu(111), this distance was reported to be 1.62 nm [30] which demonstrates the strong substrate influence on the adsorption geometry. The energetically most stable locations of the Ag bridging atoms are the 4-fold hollow sites at the center of the Ag(100) reduced unit cell.

In the OGM chain, they occupy approximately every 4th position with a distance of 4*aAg = 1.632 nm where a_{Ag} is the

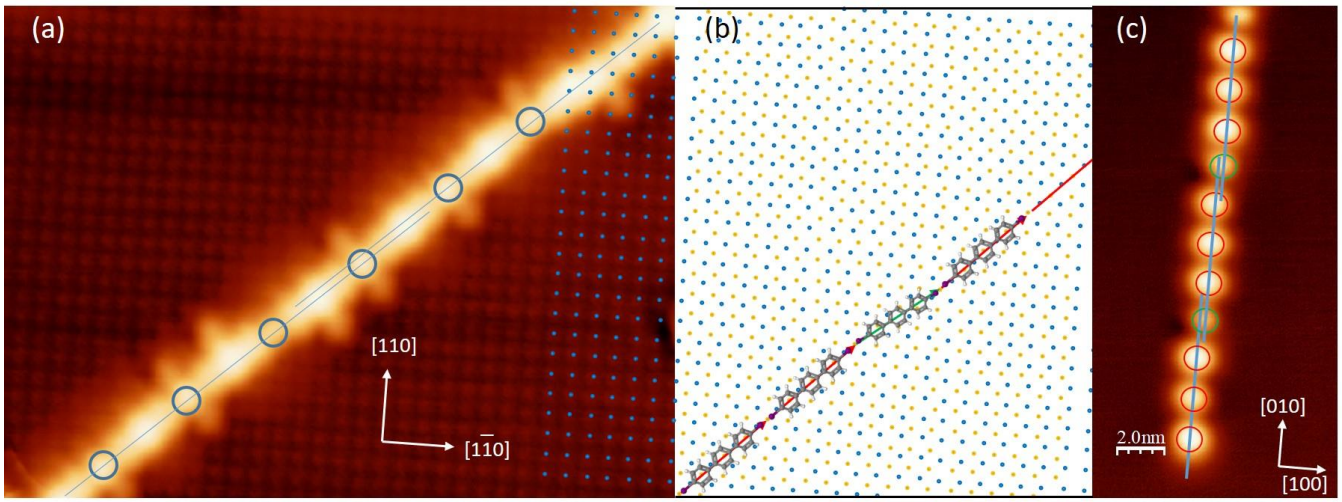

Figure 3: (a) Current constant STM images of OGM chain on Ag(100) with atomic resolution on Ag(100) together with OGM chain allowing to locate precisely the Ag bridging atom and the main crystallographic directions of the substrate (imaging conditions: 10pA, 100 mV). (b) Schematic representation of OGM wires along the [100] direction of the silver substrate presenting a tilted molecule explaining the misalignment of the chain with a jump of half unit cell. (c) Current constant STM images of OGM chain on Ag(100) recorded at 1.9V where the tilted monomer appear with a different brightness revealing a change of the LUMO state associated with a different adsorption site and bonding. Imaging conditions:1.9V, 3pA.

lattice constant of the Ag(100) face centered cubic single crystal. Every fourth monomer is therefore tilted in order to compensate the remaining mismatch of 0.036 nm between the stretched molecular length and the lattice parameters of the substrate (fig. 3b). In long chains, it might necessarily result in dislocations or chain disruptions to reduce strain and to allow relocation of Ag atoms and $(Ph)_3$. The distance between.the blue lines drawn in fig. 3a equal to $a_{Ag}/2$=0.144 nm corresponds to half unit cell. On various other STM images, multiples of aAg/2 are also found.

Other studies conducted on similar precursors report a bending of the outer phenyl rings toward the Ag surface caused by the C-Ag-C bonds [46]. In order to understand which are the parameters governing the reaction and the effect of light exposition on the different stages of PPP formation, a comparison of the temperatures required for each step of the Ullmann coupling was carried out with and without light on both Ag(100) and In the OGM chain, they occupy approximately every 4th position with a distance of 4*a_{Ag} = 1.632 nm where a_{Ag} is the lattice constant of the Ag(100) face centered cubic single crystal. Every fourth monomer is therefore tilted in order to compensate the remaining mismatch of 0.036 nm between the stretched molecular length and the lattice parameters of the substrate (fig. 3b). In long chains, it might necessarily result in dislocations or chain disruptions to reduce strain and to allow relocation of Ag atoms and $(Ph)_3$. The distance between the blue lines drawn in fig. 3a corresponds to half unit cell equal to $a_{Ag}/2$=0.144 nm. On various other STM images, multiples of $a_{Ag}/2$ are also found. Other studies conducted on similar precursors report a bending of the outer phenyl rings toward the Ag surface caused by the C-Ag-C bonds.

In order to understand which are the parameters governing the reaction and the effect of light exposition on the different stages of PPP formation, a comparison of the temperatures required for each step of the Ullmann coupling was carried out with and without light on both Ag(100) and Ag(110) surfaces. The main results are summarized in table I.

Ag	Light	300 K	373K	423K	473K	523K
100	ON	OGM	OGM	Olig,+ PPP	PPP	
	-	WM	OGM	OGM	Olig. + PPP	PPP
111	ON	OGM	PPP			
	-	OGM	Olig.	PPP		

Table I: Synthetic view of the results obtained on Ag(100) and Ag(111) at different annealing temperatures with and without light exposition. As could be seen directly from this table, the different steps of the reaction occurred at a temperature lowered by 50 K when a combination of light and annealing temperature was used.

To achieve only PPP islands, the temperature of annealing has to rise up to 473K with light and up to 523 K without light. We can conclude that the use of light in our case allows to lower the reaction temperature by 50 K at all stages of the Ullmann reaction i.e. (i) activation of the precursors by C-Br bond cleavage, (ii) formation of the oligomers by some C-Ag bond cleavages and (iii) complete Ullmann coupling by the remaining C-Ag bond cleavage and reorientation of the PPP along the <110> axis of the Ag(100) surface. The quinoid forms inside PPP islands as shown by Yuan *et al*. [33] on Cu(111) surface were not observed instead these PPP wires adopted a planar conformation as confirmed by DFT calculation.

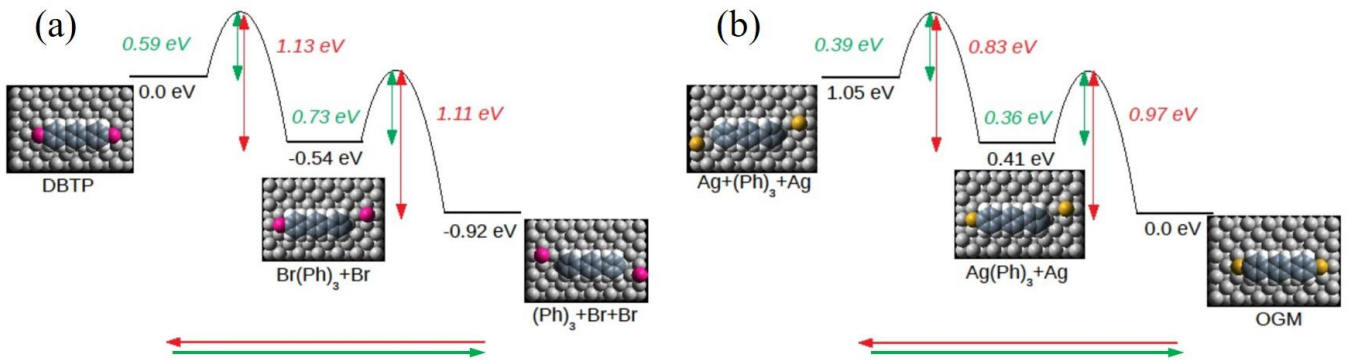

Figure 4: Energy barriers calculated by CI-NEB to overcome in order to detach (green arrow) and to attach (red arrow) (a) the first and the second bromine atoms from/to the DBTP precursors; (b) the first and the second Ag bridging atoms from/to the OGM.

Ag(111) is known to be more reactive than Ag(100), therefore, as displayed in table I, the reaction temperature stages were found to be lower than the ones on Ag(100), as expected. The interaction of DBTP with the metal surface seems to be rather weak since the same square WM arrangements of the intact molecules were found on this 3-fold symmetry substrate. The WM centres present alternate right and left handedness (SI. Fig4a). This is in striking contrast with respect to the 3-fold symmetry of the self-assembly precursors reconstruction that was found on Cu(111) [30]. As on Ag(100), the molecular self-ordering was bias energy driven and not stable at low bias. As mentioned previously, the stability of WM structures is ensured by the intermolecular halogen bonds as demonstrated by Chung *et al.* [47] In contrast with the OGM wires obtained on Ag(100), the OGM were not anymore aligned with the main crystallographic axes of the substrate but rather formed loops starting and ending at a step edge (SI fig. 4b). Another difference regards the location of the halogen atoms which are not anymore located around the Ag bridging atoms but besides the $(Ph)_3$ (SI fig. 4c). The PPP were achieved at 373 K using light assistance and at 423 K without light (SI fig.4d). Without light, thermal annealing duration of 15 min and longer yield the same results. In opposite, a minimum light exposition duration of 5 hours was needed to achieve PPP, which is partly due to our experimental setup, since at the exit of the optical fibre, the intensity was measured to drop at least by a factor 10. This is worth to mention that ordering was largely improved by the use of light with respect to only heat specially on Ag(111) as already reported in Basagni *et al.* [48] on 5,11-di-bromotetracene on Au(111). The comparison between thermal and light dissociation has shown that at 410 K, thermal process yields disordered area with rare zones where OGM dimers were observed while a significant increase of surface order was obtained by using milder conditions (room temperature) together with 405 nm light irradiation. In order to better understand, the energy barriers at play in this process, DFT calculations were carried out. The diffusion barrier calculated by using the Climbed Image-Nudge EB method shows a relatively small value of 0.172 eV and 0.171 eV for DITP and DBTP molecules respectively. These values explain the free diffusion of these molecules even at relatively low temperature of 78 K. Debromination follows a two-step process as depicted in fig. 4a. To detach the first bromine atom from the DBTP molecule adsorbed along the <100> direction, the energy to overcome the barrier was estimated to 0.59 eV. The detachment of the second Br atom requires a higher energy of 0.73 eV (fig. 4a). To provide enough energy to overcome these debromination barriers, an annealing of the substrate at 373 K was therefore necessary. The detached bromine atoms diffuse easily as their diffusion barrier was estimated as low as 0.1 eV. Remaining at this temperature of 373 K, the thus formed para-terphenyl diradical should spontaneously coordinate with diffusive Ag adatoms to form Ag-(Ph)3-Ag chains, thanks to the low coordination barriers of 0.36 eV to attach the first Ag adatom and 0.39 eV to attach the second Ag atom. In addition, the diffusion barrier of Ag adatoms is estimated to be about 0.3 eV, which favours the approach of these atoms to the reactive terphenyl diradicals. The formation of OGM is an exothermic reaction releasing 1.05 eV. The thus formed OGM complex adsorbed along the <100> direction has a length of 1.596 nm, which is 4% shorter than the distance between surface cells (1.665 nm). This length mismatch is at the origin of the misalignment detailed in fig. 2b and fig 3a. Furthermore, the adsorption energy of OGM is -6.311 eV along <100> and -6.083 eV along <110> direction. This difference in adsorption energy could be the reason why only OGM along <100> (or <010>) are observed. Starting from the OGM structure, the C-C coupling also requires the formation of para-terphenyl diradicals. Fig. 4b shows the CI-NEB calculated the activation barrier to cleave the Ag-C coordination bond which is much higher (respectively 0.97 eV and 0.83 eV to detach the first and second Ag atom) than the energy necessary to attach Ag adatoms to this diradical (0.39 and 0.36 eV). This higher activation energy could be the reason why an annealing temperature as high as 473 K was necessary for this last step. However, a question could be raised here, which is why no

direct formation of PPP through C-C coupling immediately after the p-terphenyl diradical formation is observed. To answer this, we have calculated the diffusion barrier of the terphenyl diradical to be about 1.98 eV. Thus, the direct C-C coupling when diradicals are lying parallel along the <100> direction is strongly diffusion limited. This conclusion is at first glance in contradiction with the case of benzene radicals coupling on Ag(111) and Au(111) where no energy barrier was found to establish the C-C bonds as calculated by Borjk *et al*. [49].

However, a closer look reveals that the weak activation barrier corresponds in fact to the C-C coupling when two phenyl radicals were positioned face to face at a distance close to the C-C bond. To bring these radicals to such positions, the diffusion barrier was evaluated to be about 0.3 eV on Ag(111). In the present case of diradical, there is one radical at each extremity and the whole diradical is 3 times longer than a single phenyl radical. Such a diradical requires an activation energy to diffuse much higher than the energy required for diffusion of a coordinated species Ag-$(Ph)_3$-Ag and for the $(Ph)_3$ core. Finally, the co-existence of OGM and PPP could be explained by the competition between C-C covalent bond formation and C-Ag bond formation among the remaining diradicals which might form either PPP or OGM complexes. Therefore, to ensure 100% of the diradicals to interact to form pure C-C bonds, a substrate temperature as high as 473 K was necessary. This qualitative and quantitative DFT study fully agrees with the experimental results and provides a clear picture of the Ullmann coupling process taking place at surfaces.

From these results, a number of conclusions can be drawn. Using light in combination with annealing temperature permits the formation of OGM at 300 K. Furthermore, the catalytic activity of the Ag(100) substrate is enhanced and becomes similar to that of Cu(111). A comparative table of Ullmann coupling reaction of the brominated precursors onto various substrates is shown in table II.

Precursor	Subst.	OGM	Oligomer	PPP
DBBP [29]	Au111	No	500 K	No
DBT [49]	Au111	410 K	-	
DBTP[a]	Ag100	RT+ light	423 K+ light	473 K+ light
DBBP [29]	Ag111	RT	373 K	473K
BHydroxyBP [50]	Ag111	80 K diradical	-	RT (λ=266 nm)
DBTP [30]	Cu111	RT	393K	473K
DBBP [29]	Cu111	<RT	-	450K

Table II: Comparative table of on-surface Ullmann reaction temperatures on different substrates. ([a]) refers to this work. For the same DBTP precursors, the use of light enhances the catalytic activity of the Ag(100) to Cu(111) level.

Moreover, X-ray Photoemission Spectroscopy (XPS) analysis has revealed coverage decrease due to thermal treatment while the disorder was assigned to molecular fragmentation. Another study carried out on 4-bromo-4' hydroxybiphenyl on Ag(111) has shown that upon radiation using a 266 nm UV laser at 80 K, debromination and dihydroxylation were achieved giving rise to covalently bonded polyphenylene polymer chains after annealing at RT [50]. Other photoinduced reactions involving C–X (X=Br, Cl) bond breaking have been also used as a direct route to form covalent bonding between molecular bilayers on the Si(111)-(7×7) surface [51]. In all these studies, light effect was studied only on the first step of the Ullmann reaction regarding C-X bond cleavage. Here, we have used light combined with temperature at each stage of the reaction to benefit from milder conditions. This strategy allows as well to decouple the diffusion step (activated by temperature) from the bond cleavage.

Regarding the mechanism of the photochemical effect, shining light on solids to activate surfaces has been used for the last 40 years, in particular in the domain of catalysis to enhance activity or selectivity properties of metals or oxides towards more effective dissociation of small molecules such as oxygen or water [52,53]. The mechanisms at play involve different processes, either direct photon absorption by the adsorbates, or photon absorption by the substrate, or a combination of both of them. Then, in case of direct absorption by the adsorbate, electronic excitation might decay into photon emission, vibrational states de-excitation or through other de-excitation channels opened by the presence of the substrate [53]. When the photons are absorbed by the substrate, different phenomena might occur such as photoelectrons emission, surface plasmon excitation, surface phonon, electron-hole creation and subsequent electron transfer to the adsorbate giving rise to negative ion resonances (NIRs) [54–56]. The main advantage to use light instead of heat is to favor the polymerization process under milder conditions, but also to enhance selectivity promoting only certain chemical reactions.

In this study, due to the interaction between precursors and metal, direct excitation of the vibrational transitions of DBTP or (Ag-Ph)n through light absorption can be readily discarded since it would relax faster into the heat bath provided by the substrate than into energy transfer to the low frequency molecule surface mode required for bond dissociation. In the same way, short-lived electronic excitation of the adsorbate decays into the molecule-surface vibration. However, due to short lifetimes, only a small fraction of the excited molecules, would gain sufficient energy to allow bond cleavage. Therefore, the dissociation of molecular bonds by direct adsorbate excitation occurs very rarely on metal surfaces. The origin of electronic excitation short lifetimes lies in the strong coupling of the adsorbate excited states with the nearly infinite number of electron-hole pair states provided by the substrate. Therefore, on metallic flat surfaces, the direct photoexcitation channel of the adsorbate is quenched [57,58]. From these

considerations, we can conclude that the underlying mechanism of light effect on the temperatures at which occurs the different bond cleavages could not be explained by a direct photon absorption exciting either vibrational or electronic transitions of DBTP and $(Ag\text{-}Ph)_n$ groups.

The mechanism with the highest cross section and thus more likely to occur upon light irradiation is plasmon excitation [59–61]. Resonant optical excitation of the metal surface plasmon produces hot electrons that facilitate chemical reactions. Two processes might concomitantly occur (i) when hot electrons have energy enough to directly populate the LUMO states of the adsorbate, they transfer, in our case, into the antibonding state of the C-Br bond producing the bond cleavage (ii) if hot electrons do not have energy enough to induce a direct electronic excitation, they might result in bond dissociation depending on the cumulated vibrational energy by thermal effect. This latter will induce an increase of the sample temperature which should be reflected in the temperature measurement. This hot electron mediated mechanism is supported by numerous examples where the initial photoexcitation of the substrate produces hot electrons that scatter into the molecular resonance state, leading to the dissociation of the adsorbate [59,62,63].

As pointed out in Barragán *et al*. [64] , heating induced by vibrational modes plays a negligible role in bond dissociation with respect to electronic population of the C-Br* antibonding state whenever the electron energy is high enough [65]. Spatially, photon absorption extends over the range of the penetration depth of the incoming light. The electron mean free path, which depend on the electron energy, is of the same order. Therefore, the initial hot electrons, created by photon absorption, will reach the surface with high probability. On metallic surfaces, the penetration depth of photons with an energy of a few eV is in the order of ~ 10nm, corresponding to the electron mean free path at this energy [52]. The hot electron generation phenomenon appears to be correlated with localized surface plasmon resonance enhancing the life time of these hot carriers to convert them into an efficient pathway for photochemistry on metal surfaces or semiconductor metal heterojunctions [52,53,58,59]. The hot electrons created by metal photon absorption might then tunnel into the LUMO state of the molecules forming thus a transient anion by “Hot Electron attachment” (HEA) that leads to intramolecular bond dissociation, by “Dissociative Electron Attachment” (DEA). In addition, in noble metals as Ag, strong plasmon resonances arising from the Drude-like property of sp-electrons enhance HEA efficiency. An angle-resolved high-resolution electron-energy-loss-spectroscopy (AR-HREELS) electron study reports on a single loss energy observed at 3.69 eV on Ag(100) [66], corresponding to a wavelength of 336 nm. The Xe-arc discharge lamp used in this study covers a wide range of wavelength rendering surface plasmon excitation and hot carrier generation highly probable to occur. To conclude this discussion, the temperature of the different reaction stages is most probably reduced by 50 K with respect to purely thermal processes through photon absorption by the Ag(100) substrate generating hot electrons whose lifetime is enhanced by surface plasmon excitation occurring through the same photon absorption process.

3. Conclusion

In summary, a detailed study of light assisted Ullmann reaction at Ag(100) surface was carried out starting from DBTP precursors. We found that the temperature at each stage was reduced by 50 K upon light exposition for each stage of the reaction including debromination, C-Ag bond cleavage of the OGM intermediate to achieve oligomers and finally PPP wires. The energy barriers to overcome were calculated by DFT and explained the experimental results. The underlying mechanism of light was explained by hot electron generation supported by surface plasmon excitation through photon absorption by the metallic substrate. A better ordering of the intermediate and final products was found when light was used. This original method to lower the reaction temperature provides an additional parameter to better control on-surface-synthesis by separating the activation phase from the diffusion occurring at the same time in case of purely thermal activation. This approach could be extended to other systems in particular for fragile precursors to avoid desorption or undesired fragmentation.

Acknowledgments

We acknowledge the support of the CALMIP computer center.

References

[1] Friedrich K, Sue H J, Liu P and Almajid A A 2011 Scratch resistance of high performance polymers *Tribology International* **44** 1032–46

[2] Pavlović D and Cohen S 2020 Controlled synthesis of unsubstituted high molecular weight poly(*para* -phenylene) *via* Suzuki polycondensation-thermal aromatization methodology *Polym. Chem.* **11** 2550–8

[3] Remmers M, Müller B, Martin K, Räder H-J and Köhler W 1999 Poly(*p* -phenylene)s. Synthesis, Optical Properties, and Quantitative Analysis with HPLC and MALDI−TOF Mass Spectrometry *Macromolecules* **32** 1073–9

[4] Abdulkarim A, Hinkel F, Jänsch D, Freudenberg J, Golling F E and Müllen K 2016 A New Solution to an Old Problem: Synthesis of Unsubstituted Poly(*para* -phenylene) *J. Am. Chem. Soc.* **138** 16208–11

[5] Wang T and Zhu J 2019 Confined on-surface organic synthesis: Strategies and mechanisms *Surface Science Reports* **74** 97–140

[6] Clair S and de Oteyza D G 2019 Controlling a Chemical Coupling Reaction on a Surface: Tools and Strategies for On-Surface Synthesis *Chem. Rev.* **119** 4717–76

[7] Shen Q, Gao H-Y and Fuchs H 2017 Frontiers of on-surface synthesis: From principles to applications *Nano Today* **13** 77–96
[8] Sun Q, Zhang R, Qiu J, Liu R and Xu W 2018 On-Surface Synthesis of Carbon Nanostructures *Adv. Mater.* **30** 1705630
[9] Méndez J, López M F and Martín-Gago J A 2011 On-surface synthesis of cyclic organic molecules *Chem. Soc. Rev.* **40** 4578
[10] Di Giovannantonio M, El Garah M, Lipton-Duffin J, Meunier V, Cardenas L, Fagot Revurat Y, Cossaro A, Verdini A, Perepichka D F, Rosei F and Contini G 2013 Insight into Organometallic Intermediate and Its Evolution to Covalent Bonding in Surface-Confined Ullmann Polymerization *ACS Nano* **7** 8190–8
[11] Dong L, Liu P N and Lin N 2015 Surface-Activated Coupling Reactions Confined on a Surface *Acc. Chem. Res.* **48** 2765–74
[12] Björk J and Hanke F 2014 Towards Design Rules for Covalent Nanostructures on Metal Surfaces *Chem. Eur. J.* **20** 928–34
[13] Zuzak R, Jančařík A, Gourdon A, Szymonski M and Godlewski S 2020 On-Surface Synthesis with Atomic Hydrogen *ACS Nano* **14** 13316–23
[14] Fan Q, Dai J, Wang T, Kuttner J, Hilt G, Gottfried J M and Zhu J 2016 Confined Synthesis of Organometallic Chains and Macrocycles by Cu–O Surface Templating *ACS Nano* **10** 3747–54
[15] Nacci C, Viertel A, Hecht S and Grill L 2016 Covalent Assembly and Characterization of Nonsymmetrical Single-Molecule Nodes *Angew. Chem. Int. Ed.* **55** 13724–8
[16] Cirera B, Zhang Y-Q, Björk J, Klyatskaya S, Chen Z, Ruben M, Barth J V and Klappenberger F 2014 Synthesis of Extended Graphdiyne Wires by Vicinal Surface Templating *Nano Lett.* **14** 1891–7
[17] de Oteyza D G, Gorman P, Chen Y-C, Wickenburg S, Riss A, Mowbray D J, Etkin G, Pedramrazi Z, Tsai H-Z, Rubio A, Crommie M F and Fischer F R 2013 Direct Imaging of Covalent Bond Structure in Single-Molecule Chemical Reactions *Science* **340** 1434–7
[18] Treier M, Pignedoli C A, Laino T, Rieger R, Müllen K, Passerone D and Fasel R 2011 Surface-assisted cyclodehydrogenation provides a synthetic route towards easily processable and chemically tailored nanographenes *Nature Chem* **3** 61–7
[19] Aragonès A C, Haworth N L, Darwish N, Ciampi S, Bloomfield N J, Wallace G G, Diez-Perez I and Coote M L 2016 Electrostatic catalysis of a Diels–Alder reaction *Nature* **531** 88–91
[20] Gong Z, Yang B, Lin H, Tang Y, Tang Z, Zhang J, Zhang H, Li Y, Xie Y, Li Q and Chi L 2016 Structural Variation in Surface-Supported Synthesis by Adjusting the Stoichiometric Ratio of the Reactants *ACS Nano* **10** 4228–35
[21] Domínguez-Celorrio A, Vilas-Varela M, Peña D, Langlais V and Serrate D 2021 Symmetry-Driven Formation of Chiral Boroxine-Based Organometallic Oligomers on Ag(001) *J. Phys. Chem. C* **125** 2015–21
[22] Piantek M, Serrate D, Moro-Lagares M, Algarabel P, Pascual J I and Ibarra M R 2014 Manganese Phthalocyanine Derivatives Synthesized by On-Surface Cyclotetramerization *J. Phys. Chem. C* **118** 17895–9
[23] Liu M, Chen S, Li T, Wang J and Zhong D 2018 Tuning On-Surface Synthesis of Graphene Nanoribbons by Noncovalent Intermolecular Interactions *J. Phys. Chem. C* **122** 24415–20
[24] Cai J, Ruffieux P, Jaafar R, Bieri M, Braun T, Blankenburg S, Muoth M, Seitsonen A P, Saleh M, Feng X, Müllen K and Fasel R 2010 Atomically precise bottom-up fabrication of graphene nanoribbons *Nature* **466** 470–3
[25] Zuzak R, Dorel R, Kolmer M, Szymonski M, Godlewski S and Echavarren A M 2018 Higher Acenes by On-Surface Dehydrogenation: From Heptacene to Undecacene *Angew. Chem. Int. Ed.* **57** 10500–5
[26] Di Giovannantonio M and Contini G 2018 Reversibility and intermediate steps as key tools for the growth of extended ordered polymers via on-surface synthesis *J. Phys.: Condens. Matter* **30** 093001
[27] Lackinger M 2017 Surface-assisted Ullmann coupling *Chem. Commun.* **53** 7872–85
[28] Lipton-Duffin J A, Ivasenko O, Perepichka D F and Rosei F 2009 Synthesis of Polyphenylene Molecular Wires by Surface-Confined Polymerization *Small* **5** 592–7
[29] Zhou X, Bebensee F, Shen Q, Bebensee R, Cheng F, He Y, Su H, Chen W, Xu G Q, Besenbacher F, Linderoth T R and Wu K 2017 On-surface synthesis approach to preparing one-dimensional organometallic and poly-p-phenylene chains *Mater. Chem. Front.* **1** 119–27
[30] Wang W, Shi X, Wang S, Van Hove M A and Lin N 2011 Single-Molecule Resolution of an Organometallic Intermediate in a Surface-Supported Ullmann Coupling Reaction *J. Am. Chem. Soc.* **133** 13264–7
[31] Jang W J, Chung K-H, Lee M W, Kim H, Lee S and Kahng S-J 2014 Tetragonal porous networks made by rod-like molecules on Au(111) with halogen bonds *Applied Surface Science* **309** 74–8
[32] Basagni A, Sedona F, Pignedoli C A, Cattelan M, Nicolas L, Casarin M and Sambi M 2015 Molecules–Oligomers–Nanowires–Graphene Nanoribbons: A Bottom-Up Stepwise On-Surface Covalent Synthesis Preserving Long-Range Order *J. Am. Chem. Soc.* **137** 1802–8
[33] Yuan B, Li C, Zhao Y, Gröning O, Zhou X, Zhang P, Guan D, Li Y, Zheng H, Liu C, Mai Y, Liu P, Ji W, Jia J and Wang S 2020 Resolving Quinoid Structure in Poly(*para* -phenylene) Chains *J. Am. Chem. Soc.* **142** 10034–41
[34] Song S, Kojima T, Nakae T and Sakaguchi H 2017 Wide graphene nanoribbons produced by interchain fusion of poly(p-phenylene) via two-zone chemical vapor deposition *Chem. Commun.* **53** 7034–6
[35] Fan Q, Wang C, Han Y, Zhu J, Hieringer W, Kuttner J, Hilt G and Gottfried J M 2013 Surface-Assisted Organic Synthesis of Hyperbenzene Nanotroughs *Angew. Chem. Int. Ed.* **52** 4668–72
[36] Judd C J, Haddow S L, Champness N R and Saywell A 2017 Ullmann Coupling Reactions on Ag(111) and Ag(110); Substrate Influence on the Formation of Covalently Coupled Products and Intermediate Metal-Organic Structures *Sci Rep* **7** 14541
[37] Kresse G and Furthmüller J 1996 Efficiency of ab-initio total energy calculations for metals and semiconductors using a plane-wave basis set *Computational Materials Science* **6** 15–50

[38] Kresse G and Furthmüller J 1996 Efficient iterative schemes for *ab initio* total-energy calculations using a plane-wave basis set *Phys. Rev. B* **54** 11169–86
[39] Blöchl P E 1994 Projector augmented-wave method *Phys. Rev. B* **50** 17953–79
[40] Perdew J P, Burke K and Ernzerhof M 1996 Generalized Gradient Approximation Made Simple *Phys. Rev. Lett.* **77** 3865–8
[41] Grimme S 2006 Semiempirical GGA-type density functional constructed with a long-range dispersion correction *J. Comput. Chem.* **27** 1787–99
[42] Henkelman G, Uberuaga B P and Jónsson H 2000 A climbing image nudged elastic band method for finding saddle points and minimum energy paths *The Journal of Chemical Physics* **113** 9901–4
[43] Henkelman G and Jónsson H 2000 Improved tangent estimate in the nudged elastic band method for finding minimum energy paths and saddle points *The Journal of Chemical Physics* **113** 9978–85
[44] Cavallo G, Metrangolo P, Milani R, Pilati T, Priimagi A, Resnati G and Terraneo G 2016 The Halogen Bond *Chem. Rev.* **116** 2478–601
[45] Calupitan J P D C, Galangau O, Guillermet O, Coratger R, Nakashima T, Rapenne G and Kawai T 2017 Scanning Tunneling Microscope Tip-Induced Formation of a Supramolecular Network of Terarylene Molecules on Cu(111) *J. Phys. Chem. C* **121** 25384–9
[46] Kawai S, Sadeghi A, Okamoto T, Mitsui C, Pawlak R, Meier T, Takeya J, Goedecker S and Meyer E 2016 Organometallic Bonding in an Ullmann-Type On-Surface Chemical Reaction Studied by High-Resolution Atomic Force Microscopy *Small* **12** 5303–11
[47] Chung K-H, Park J, Kim K Y, Yoon J K, Kim H, Han S and Kahng S-J 2011 Polymorphic porous supramolecular networks mediated by halogen bonds on Ag(111) *Chem. Commun.* **47** 11492
[48] Basagni A, Ferrighi L, Cattelan M, Nicolas L, Handrup K, Vaghi L, Papagni A, Sedona F, Valentin C D, Agnoli S and Sambi M 2015 On-surface photo-dissociation of C–Br bonds: towards room temperature Ullmann coupling *Chem. Commun.* **51** 12593–6
[49] Björk J, Hanke F and Stafström S 2013 Mechanisms of Halogen-Based Covalent Self-Assembly on Metal Surfaces *J. Am. Chem. Soc.* **135** 5768–75
[50] Shen Q, He J H, Zhang J L, Wu K, Xu G Q, Wee A T S and Chen W 2015 Self-assembled two-dimensional nanoporous molecular arrays and photoinduced polymerization of 4-bromo-4′-hydroxybiphenyl on Ag(111) *The Journal of Chemical Physics* **142** 101902
[51] Zhang Y P, He J H, Xu G Q and Tok E S 2012 Architecturing Covalently Bonded Organic Bilayers on the Si(111)-(7 × 7) Surface via in Situ Photoinduced Reaction *J. Phys. Chem. C* **116** 8943–9
[52] Hasselbrink E 1994 Mechanisms in photochemistry on metal surfaces *Applied Surface Science* **79–80** 34–40
[53] Franchy R 1998 Surface and bulk photochemistry of solids *Rep. Prog. Phys.* **61** 691–753
[54] Engel F, Dieterle T, Hummel F, Fey C, Schmelcher P, Löw R, Pfau T and Meinert F 2019 Precision Spectroscopy of Negative-Ion Resonances in Ultralong-Range Rydberg Molecules *Phys. Rev. Lett.* **123** 073003
[55] Illenberger E 2003 Formation and evolution of negative ion resonances at surfaces *Surface Science* **528** 67–77
[56] Marinica D C, Ramseyer C, Teillet-Billy D and Gauyacq J P 2006 Negative ion resonance of a molecule adsorbed on a metal surface covered with a rare gas monolayer *Surface Science* **600** 803–14
[57] Kim M, Lin M, Son J, Xu H and Nam J-M 2017 Hot-Electron-Mediated Photochemical Reactions: Principles, Recent Advances, and Challenges *Advanced Optical Materials* **5** 1700004
[58] Zhang Y, He S, Guo W, Hu Y, Huang J, Mulcahy J R and Wei W D 2018 Surface-Plasmon-Driven Hot Electron Photochemistry *Chem. Rev.* **118** 2927–54
[59] Brongersma M L, Halas N J and Nordlander P 2015 Plasmon-induced hot carrier science and technology *Nature Nanotech* **10** 25–34
[60] Christopher P, Xin H and Linic S 2011 Visible-light-enhanced catalytic oxidation reactions on plasmonic silver nanostructures *Nature Chem* **3** 467–72
[61] Liu J, Cai Z-Y, Sun W-X, Wang J-Z, Shen X-R, Zhan C, Devasenathipathy R, Zhou J-Z, Wu D-Y, Mao B-W and Tian Z-Q 2020 Plasmonic Hot Electron-Mediated Hydrodehalogenation Kinetics on Nanostructured Ag Electrodes *J. Am. Chem. Soc.* **142** 17489–98
[62] Lee J, Ryu J, Kim S and Kim S K Direct Observation of an Intermediate State for a Surface Photochemical Reaction Initiated by Hot Electron Transfer *J. Phys. Chem. B 2005, 109, 30*
[63] Palmino F, Loppacher C and Chérioux F 2019 Photochemistry Highlights on On-Surface Synthesis *ChemPhysChem* **20** 2271–80
[64] Barragán A, Robles R, Lorente N and Vitali L 2021 Power discontinuity and shift of the energy onset of a molecular de-bromination reaction induced by hot-electron tunneling *Nanoscale* 10.1039.D1NR04229G
[65] Erpenbeck A, Ke Y, Peskin U and Thoss M 2020 Current-induced dissociation in molecular junctions beyond the paradigm of vibrational heating: The role of antibonding electronic states *Phys. Rev. B* **102** 195421
[66] Rocca M, Biggio F and Valbusa U 1990 Surface-plasmon spectrum of Ag(001) measured by high-resolution angle-resolved electron-energy-loss spectroscopy *Phys. Rev. B* **42** 2835–41